Available online at www.sciencedirect.com
ScienceDirect
C. R. Physique 8 (2007) 69–84
COMPTES RENDUS PHYSIQUE
http://france.elsevier.com/direct/COMREN/

Observation of black holes and extreme gravitational events/Observation des trous noirs et des événements gravitationnels extrêmes

Optical detection of gravitational waves

Jean-Yves Vinet

ARTEMIS, observatoire de la côte d'Azur, B.P. 4229, 06304 Nice cedex 04, France

Available online 2 February 2007

Abstract

We present the fundamentals of gravitational wave antennas in the high frequency domain (ground based detectors) and in the low frequency domain (space antenna). We then discuss the main technological challenges, the fundamental limits and the present status. ***To cite this article: J.-Y. Vinet, C. R. Physique 8 (2007).***

Résumé

Sur la détection optique des ondes de gravitation. On présente d'abord les principes de base des antennes gravitationnelles dans les domaines haute fréquence (instruments terrestres) et basse fréquences (antennes spatiales), on discute ensuite les principaux défis technologiques qui ont été relevés, les limites fondamentales, et l'état présent des projets en cours. ***Pour citer cet article : J.-Y. Vinet, C. R. Physique 8 (2007).***

Keywords: Gravitational waves; Optical detection

Mots-clés : Ondes de gravitation ; Détection optique

1. Introduction

Observation of the Universe reveals more and more highly relativistic objects, even in our galaxy. Most of these objects involve neutron stars and/or black holes of various masses. Different electromagnetic observation channels (optical, X-rays, ...) have already given well-known exciting pictures. A deeper understanding of the dynamics of systems of black holes and of the formation of supermassive black holes should be obtained from extra channels, including gravitational radiation. Ground based detectors of Gravitational Waves (GW) have been built in the US (the two LIGOs), in Europe (GEO600 and Virgo) and in Japan (TAMA) for studying compact inspiralling binaries of stellar masses, including black hole binaries of several tens of solar masses. The gravitational frequencies of the GW emitted during such events overlap the sensitivity band of terrestrial GW antennas (from a few Hz to a few kHz). We shall review the various technological challenges encountered during the R&D period, and the present status. Supermassive black holes (SMBH) may exist as systems (e.g. binaries) or as single attractors capturing neighbouring smaller objects. The frequency range for GW produced directly or indirectly by SMBH is under the Hz. Only a space

E-mail address: Jean-Yves.Vinet@obs-nice.fr.

1631-0705/$ – see front matter
doi:10.1016/j.crhy.2006.11.003

antenna free from terrestrial seismic motion can address this frequency domain. The LISA project aims to detect GW from a fraction of mHz to a fraction of Hz. We shall discuss the basic ideas of LISA.

2. Physics of gravitational waves

2.1. Emission

Gravitational waves (GW) are a consequence of Einstein's General Relativity (GR), just as electromagnetic waves come from Maxwell's Electrodynamics. In the framework of Special Relativity, in a system of coordinates x^λ, an electromagnetic wave is described (in vacuum) by the vector field $A_\mu(x^\lambda)$ (4-potential) obeying the Maxwell equations. The wave propagates at velocity c, is transverse and has two polarization components. In GR, the gravitational state of spacetime is associated to its geometry through the metric tensor $g_{\mu\nu}(x^\lambda)$ obeying the Einstein equations. In the case of a gravitational wave far from its source, in a freely falling reference system, one can write:

$$g_{\mu\nu}(t,\mathbf{x}) = \eta_{\mu\nu} + h_{\mu\nu}(t,\mathbf{x}) \tag{1}$$

where $\eta_{\mu\nu} \equiv \mathrm{diag}(1,-1,-1,-1)$ is the Minkowski tensor of the locally flat background spacetime (freely falling frame), and $h_{\mu\nu}$ a very small dimensionless tensor field representing the GW amplitude. It can be shown that $h_{\mu\nu}$ can be eventually reduced to only two independent functions $h_+, h_\times$ defining the polarization state of the wave. Gravitational waves are emitted by distributions of matter/energy having a time dependent quadrupole moment. In the transverse-traceless gauge, only the space components are significant and we have in the so-called TT-gauge, an expression analogous to a retarded potential [1]:

$$h_{jk}(t,r) = \frac{2G}{c^4}\frac{1}{r}\partial_t^2\big[\Xi_{jk}(t-r/c)\big]^{TT} \tag{2}$$

($r \equiv \mathbf{x}^2$), where the symmetric trace-free quadrupole tensor $\Xi(t)$ is defined by the volume integral:

$$\Xi_{jk}(t) = \int \rho(t,\mathbf{x})\left[x^i x^j - \frac{1}{3}\delta_{jk}\mathbf{x}^2\right]\mathrm{d}^3x$$

where ρ is the density of matter. One immediately notes the extreme weakness of the coupling coefficient G/c^4 which is the cause of all technological challenges encountered on the way to GW astronomy. Only astrophysical events involving stars or black holes in the nearly relativistic velocity regime can cause amplitudes of GW larger than 10^{-25} in the neighborhood of the Earth. The most promising candidates are the final inspiralling of compact binaries. The frequency domain of the waves is determined by the masses of the components of the binary. Stellar class binaries can end at 1 kHz whereas Massive Black Holes can end at a small fraction of a Hz. The observation instruments must change according to the addressed domain of frequency. Existing instruments have been designed for a sensitivity of about 10^{-23} at the middle of the bandwidth, which seemed the best feasible in the 1980s, when the R&D studies ended.

2.2. Physical effects of a GW

Being a perturbation of the geometry of spacetime, one can expect a GW to produce distortions in some metrology experiments. We briefly recall the existence of narrow band solid antennas, then focus on optical experiments.

2.2.1. Resonant detectors

The first proposed experiment [2] rested on the idea that a GW could induce stresses in solids, and that on a suitably isolated solid resonator, weakly dissipative for acoustic waves, one could detect with some transducer system the resonances occurring when the GW signal overlaps its acoustical bandwidth. This idea is supported by a general relativistic extension of the linear elasticity theory [3]. A result is the modified tensor elastodynamic equation:

$$\rho\ddot{E}_{ij} - \frac{1}{2}[\partial_k\partial_j\Theta_{ik} + \partial_k\partial_i\Theta_{jk}] = -\frac{1}{2}\rho\ddot{h}_{ij} \tag{3}$$

where E_{ij} and Θ_{ij} are the classical strain and stress tensors, respectively, and ρ the density. If we take the origin of coordinates at the center of mass, and if we assume a GW wavelength much larger than the size of the resonator, this can be regarded as a derivative of the vector elastodynamic equation:

$$\rho\ddot{u}^i - \partial_k \Theta^{ik} = -\frac{1}{2}\rho\ddot{h}^{ij}x^j \tag{4}$$

where **u** is the displacement vector. The GW amplitude appears thus as a driving internal (of tidal type) force acting on the resonator. After the controversial but negative results of Weber, several groups nevertheless built hugely improved versions of the Weber antenna. These instruments called 'bar antennas' have been built in several countries [4,5], and even larger resonators having spherical shapes are planned [6].

2.2.2. Optical detectors

A more direct physical effect of GW is to modulate the light distances between freely falling test masses. In vacuum, light is expected to propagate along a null geodesic, which means that the invariant element of spacetime $\mathrm{d}s^2 \equiv g_{\mu\nu}\,\mathrm{d}x^\mu\,\mathrm{d}x^\nu$ is identically zero along any optical path. With the expression (1) of the metric tensor, one can suspect that the effective optical paths of photons will be perturbed.

2.2.2.1. Detectors of size much smaller than the GW wavelength. The expected frequencies of GW events for obvious reasons are much lower (at most a few kHz) than optical frequencies. In this regime, the only effect of a GW on light is to perturb the flight time of photons between two test masses (light distances). Consider a light path lying in the (x, y) plane, either along the x (north) or the y (west) axis. Consider, on the other hand, a GW propagating along a direction of unit vector **w**.

$$\mathbf{w} = \begin{pmatrix} \sin\theta\cos\phi \\ \sin\theta\sin\phi \\ \cos\theta \end{pmatrix} \tag{5}$$

If $h_+, h_\times$ are the two polarization components of the wave, the effect of the GW is to create a phase modulation on the two beams:

$$\Phi_{\text{north}}(t) = \frac{2\pi L}{\lambda}\left[h_+(t)\left(\cos^2\theta\cos^2\phi - \sin^2\phi\right) - h_\times(t)\cos\theta\sin 2\phi\right] \tag{6}$$

$$\Phi_{\text{west}}(t) = \frac{2\pi L}{\lambda}\left[h_+(t)\left(\cos^2\theta\sin^2\phi - \cos^2\phi\right) + h_\times(t)\cos\theta\sin 2\phi\right] \tag{7}$$

In an interferometric configuration, where the observable is a differential phase, this gives:

$$\Delta\Phi(t) = \frac{4\pi L}{\lambda}\left[h_+(t)\frac{1+\cos^2\theta}{2}\cos 2\phi - h_\times(t)\cos\theta\sin 2\phi\right] \tag{8}$$

where it can be seen that the interferometer acts like a transducer, converting the gravitational signal into a phase and eventually into an electrical signal through some photo detector.

2.2.2.2. Detectors of size comparable to the GW wavelength. In the case of very long range optical paths (e.g. 5 Mkm in the case of LISA), one must take into account the action of the GW during light propagation. If a light beam of fixed frequency is emitted from A and detected at B, the nominal distance AB being L and **n** the unit vector from A to B, the physical effect detected at B is a frequency modulation. Let **w** be again the propagation unit vector of the GW, and let us define two more unit vectors mutually orthogonal in the transverse plane:

$$\vartheta = \frac{\partial\mathbf{w}}{\partial\theta}, \qquad \varphi = \frac{1}{\sin\theta}\frac{\partial\mathbf{w}}{\partial\phi}$$

then the two directional functions

$$\xi_+(\theta,\phi) = (\vartheta.\mathbf{n})^2 - (\varphi.\mathbf{n})^2, \qquad \xi_\times(\theta,\phi) = 2(\vartheta.\mathbf{n})(\varphi.\mathbf{n})$$

then the function

$$H(t) = h_+(t)\xi_+(\theta,\phi) + h_\times\xi_\times(\theta,\phi) \tag{9}$$

Now the observable is a relative frequency modulation, analogous to a Doppler shift [7] given by ($c = 1$):

$$\left[\frac{\delta\nu(t)}{\nu}\right]_{A\to B} = \frac{H(t - \mathbf{w}.\mathbf{x}_B) - H(t - \mathbf{w}.\mathbf{x}_A - L)}{2(1 - \mathbf{w}.\mathbf{n})} \tag{10}$$

where $\mathbf{x}_A$ and $\mathbf{x}_B$ are the positions of the two. This is often called a 'two pulse' response because a short GW pulse would have this double effect on a phasemeter at B.

3. Ground based detectors

3.1. General principles

3.1.1. Interferometry

A Michelson interferometer involves a splitter sharing a laser light into two secondary beams that recombine on it after a reflection on distant mirrors, generating interferences on a photodetector. Such a device generates a phase quantum (shot) noise due to the quantum nature of light detection and characterized by the white power spectral density (PSD)

$$S(f) = \frac{2\hbar\omega}{P_L}$$

where $\lambda \equiv 2\pi c/\omega$ is the laser wavelength and P_L its power. The quantum efficiency of the photodetector has been taken equal to 1. If according to (8), the differential phase induced by the GW is at most (single and optimal polarization, normal incidence):

$$\Delta\Phi(t) = \frac{4\pi L}{\lambda}h(t)$$

the result is that the ultimate, shot-noise limited sensitivity of a simple Michelson having two orthogonal arms of length L is given by the white linear spectral density (LSD):

$$S_h^{1/2} = \frac{\lambda}{4\pi L}\sqrt{\frac{2\hbar\omega}{P_L}} \tag{11}$$

It is easily seen that even with large parameters ($L = 3$ km, $P_L = 20$ W), the result ($\sim 4 \times 10^{-21}$ Hz$^{-1/2}$) is far from the requirements. It is seen, as well, that increasing these already big parameters is not so easy. Solutions have been proposed years ago by R. Drever [8].

3.1.2. Fabry–Perot cavities

The leading idea is to use the properties of resonant cavities firstly for increasing the effective lengths of the arms, and secondly for increasing the effective power reaching the splitter. Consider a resonant (Fabry–Perot) cavity of length L, having an input mirror of reflectivity r_1, an end mirror of reflectivity r_2. The relevant parameters are:

– The finesse $\mathcal{F}$ given by

$$\mathcal{F} = \frac{\pi\sqrt{r_1 r_2}}{1 - r_1 r_2} \tag{12}$$

– The free spectral range $\Delta\nu$ or frequency gap between two successive resonances:

$$\Delta\nu = \frac{c}{2L} \tag{13}$$

– The linewidth $\delta\nu$ defined by:

$$\delta\nu = \Delta\nu/\mathcal{F} \tag{14}$$

One can show that in such a cavity tuned at resonance:

– The reflectance of the cavity as a whole is:

$$r_{\text{cav}} = 1 - \sigma$$

where the coupling coefficient σ is

$$\sigma = p\mathcal{F}/\pi \tag{15}$$

p being the total relative light power loss of the cavity per round trip (thermalization, diffraction ...).

– The phase change of the reflected wave on a very tiny displacement δL of the end mirror is

$$\delta\Phi = \frac{8\mathcal{F}}{\lambda}\delta L$$

If we compare to the phase change due to the same displacement without input mirror (with only the end mirror)

$$\delta\Phi = \frac{4\pi}{\lambda}\delta L$$

we see that the cavity has an effect equivalent to $\mathcal{S} = 2\mathcal{F}/\pi$ round trips. For a finesse of 50, as currently planned, the result is equivalent, in terms of h to an arm of length $L_{\text{eff}} \sim 100$ km.

– If we compute the power P_{stored} stored at resonance we obtain as long as $\sigma \ll 1$:

$$P_{\text{stored}} = \frac{2\mathcal{F}}{\pi} P_{\text{inc}}$$

where P_{inc} is the power reaching the input mirror. Parameter $\mathcal{S} = 2\mathcal{F}/\pi$ is called surtension coefficient. It is equal to the effective number of round trips in the cavity.

3.1.3. Recycling interferometers

These interesting properties of resonant cavities are the basis of all optical GW antennas. On Fig. 1, one can see the principles of Virgo (for instance). It can be shown that the optimal sensitivity of a shot noise limited interferometer is reached when the extinction of the outgoing beam (to photodetector) is a maximum. The whole Michelson section (the two arms plus the splitter) act therefore as a virtual mirror, and adding one more mirror (the recycler) builds a new cavity, called the recycling cavity: one may imagine that the light almost totally reflected by the Michelson re-enters the interferometer. In other words, the recycler carries out an impedance matching between the laser and the Michelson. Starting from a 20 W laser, a first resonance increases to 1 kW the power reaching the splitter. After splitting, 500 W are fed into the long cavities, and the power stored in these is about 15 kW. The finesse of the arm

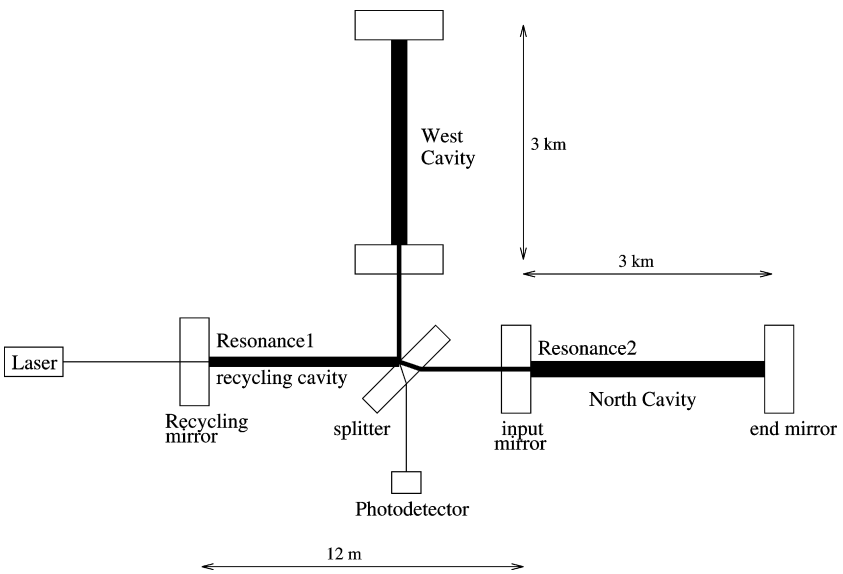

Fig. 1. Sketch of a recycling Fabry–Perot interferometer.

cavities was fixed at $\mathcal{F} = 50$, increasing the effective length of the arms by a factor of about 30 giving 90 effective km, and the surtension coefficient of the recycling cavity at $\mathcal{S} = 50$. The total gain factor with respect to a simple Michelson is better than 200 according to (11), giving a LSD of h equivalent to shot noise of about $2 \times 10^{-23}\ \mathrm{Hz}^{-1/2}$, consistent with the requirements. This spectral density is no longer white, however, because the transfer function from GW to detected phase falls to zero when the GW frequency is larger than the linewidth of the long cavities (or when the GW wavelength becomes shorter than the effective lengths of the arms as well). The complete LSD of h equivalent to shot noise is:

$$S_h^{1/2}(f) = \frac{\lambda}{8\mathcal{F}L}\sqrt{\frac{2\hbar\omega}{P_L}}\frac{1}{\sqrt{\mathcal{S}}}\sqrt{1 + 4(f/\delta\nu)^2} \tag{16}$$

Shot noise is not, however, the only fundamental limit to this kind of metrology.

3.2. The isolation challenge

There is no way to distinguish GW action on the space between mirrors and the spurious motion of these. At the level of about $10^{-20}\ \mathrm{m\,Hz}^{-1/2}$, there are numerous causes of spurious motion. There is no hope of reaching the fundamental limits without a very efficient isolation system.

3.2.1. Seismic isolation

The mirrors are suspended by thin wires in order to be almost free in the horizontal plane for small motions (approximation of free fall). All optical antennas have therefore a more or less sophisticated filtering system. The complexity of the filter depends on the fixed 'wall' frequency i.e. the lower frequency bound. For a wall at 50 Hz, classical acoustic filters, such as LIGOs, work. For pushing back the wall to 10 Hz, a more complex system was devised for Virgo. It is well known that the oscillations y of a pendulum are related to those x of its suspension point by a transfer function (TF) of the form

$$\frac{\tilde{y}(f)}{\tilde{x}(f)} = \frac{1}{1 - f^2/f_0^2}$$

where f_0 is the resonance frequency. There is thus an attenuation factor of f_0^2/f^2 for frequencies much larger than the resonance. The idea of a so-called 'superattenuator' was to construct a chain of n pendulums able to oscillate with very low resonance frequencies along all degrees of freedom (vertical and horizontal). The global TF is approximately the product of all elementary TFs, or $(f_0/f)^{2n}$ assuming comparable resonance frequencies. The pendulums are essentially heavy masses ($\sim$100 kg) suspended by 1 m long wires giving a resonance at about 0.5 Hz for the horizontal motion, and containing steel blades whose bending stiffness has been reduced by magnets (negative spring) for the vertical motion. A global attenuation factor of about 10^{-14} at 10 Hz is obtained this way.

3.2.2. Vacuum

Suppressing the refraction index fluctuations due to air pressure fluctuations requires operating in ultravacuum. The residual hydrogen pressure must be lower than 10^{-9} mbar and 10^{-14} mbar for hydrocarbons. All the optical system and the suspensions must therefore be installed in a high quality vacuum system. The steel pipelines containing the cavities have 1.2 m diameter and are 3 km long. This represents an area of about 30 000 m^2. An important and successful item in the R&D program was to find the thermal treatment of stainless steel able to suppress the outgassing rate to the required level, in order to avoid operating with continuous pumping. The external aspect of ground based detectors is determined by this huge vacuum system (see the example of Virgo on Fig. 2).

3.3. The thermal noise challenge

The second fundamental limit in the sensitivity comes from the fact that the optical system essentially reads the distance between the reflecting surfaces of two mirrors (in each cavity). It is thus clear that any spurious motion of these surfaces competes with the gravitational signal. Once eliminated inessential causes of motion (sound waves, seismic vibrations, ...) by the isolation system, there remains sources of motion in the thermal random excitation

Fig. 2. Aerial view of Virgo.

inside all material elements of the system holding the mirrors. As seen above, the filtering chain suspending the mirrors is a series of harmonic oscillators coupled with the mirror's motions. The mirrors themselves, that are thick (10 cm) and wide (35 cm diameter) silica cylinders may be considered as solid resonators and have elastodynamic modes disturbing their shapes, resulting in an apparent displacement. The resulting noise in the readout system is called thermal noise. Three different sectors of thermal noise can be distinguished:

– The thermal excitation of the pendulum chain suspending the mirror holder. The corresponding spectral density fixes the wall frequency at 10 Hz.
– The thermal excitation of the wires holding the mirrors from the last pendulum stage. The resonances of these wires are called 'violin modes'. These resonances can be sharpened by using high Q materials and weldings. The present trend is to use monolithic silica suspensions.
– The internal modes of the mirrors substrates give a PSD of noise with a low frequency tail dominating all noises in the 100 Hz region.

The region of 100 Hz being very interesting from the astrophysics point of view, a number of efforts have been spent for finding ways of reducing the mirrors thermal noise. Let us discuss the proposed ideas.

3.3.1. Cooling

The PSD of thermal noise is proportional to the temperature T, so that cooling is an obvious good idea. However, the LSD is proportional to $\sqrt{T}$ so that in order to gain 1 order of magnitude in sensitivity, one must reach cryogenic temperatures. This has been tested in the Japanese experiment but not yet in a full scale antenna.

3.3.2. New materials

More specifically it has been shown [9] that the low frequency tail of the PSD of displacement equivalent to thermal noise in the mirrors is:

$$S_x(f) = \frac{4k_B T}{\pi f}\phi U \tag{17}$$

where k_B is the Boltzmann constant, ϕ a loss angle (inverse of a quality factor) and U the strain energy stored in the solid substrate under a pressure distribution having the profile of the readout optical beam and normalized to 1 N

resulting force. The second parameter to play with is the loss angle ϕ. It seems that it is difficult to have loss angles less than 10^{-6} with synthetic silica. This is why it has been proposed to use sapphire instead. Unfortunately sapphire has bad optical properties, so that it could not be used for transmitting mirrors.

3.3.3. Beam reshaping

The third parameter on which to act is U, which leads us to look for beam profiles that decrease that (virtual) mirror strain. In the current situation, the optical beams circulating in the interferometers are the Gaussian beams emitted by standard lasers in which optical power is focused on a small spot at the center of the mirror. By substituting homogeneously distributed beams ('flat top' beams [10]) it has been shown [11] that a gain factor of about 3 could be achieved in the LSD with respect to the present situation in the Virgo input mirrors. This kind of optical mode is, however, obtained in a Fabry–Perot cavity by using non spherical mirrors. Some numerical and experimental R&D studies have been carried out [12] to test the operation of such cavity from the point of view of optical stability under small misalignments.

Recently it has been proposed [13] to use high order TEM modes, for instance Laguerre–Gauss modes of order 5 or more to obtain the required homogeneous power distribution. These modes at the same time allow a better noise reduction and keep a spherical wavefront. A gain of about 5 on the LSD of thermal noise could be attained. An important point is that ordinary spherical mirrors are still used.

3.4. The optical challenge

The shot-noise limited sensitivity of 2×10^{-23} $\mathrm{Hz}^{-1/2}$ that has been shown above theoretically feasible rests on a good reflectance of the Michelson subsystem, i.e. a reflectance allowing us to get the required surtension $\mathcal{S} \sim 50$ in the recycling cavity. It is easily seen that the maximum $\mathcal{S}$ is:

$$\mathcal{S}_{\max} = \frac{1 - p_r}{1 - (1 - p_r)(1 - p_s)^2(1 - \sigma)^2}$$

where p_r, p_s are the losses at the recycling mirror and at the splitter respectively, whereas σ is the coupling rate of the cavities defined above (15). These losses are dominated by the coupling rate (by a factor comparable to the finesse), so that a rough estimate of the maximum gain is:

$$\sqrt{\mathcal{S}_{\max}} = \frac{1}{\sqrt{2\sigma}} = \frac{1}{\sqrt{4p\mathcal{F}/\pi}}$$

To have $\mathcal{S} \geqslant 50$ with $\mathcal{F} = 50$, the overall losses must therefore be less than 300 ppm. These losses involve not only thermalization of light, but also scattering (roughness of the reflecting surfaces), diffraction (aberration) and misalignments, so that this figure of 300 ppm is demanding. Scattering losses scale as $1/\lambda^2$. A special synthetic silica has been developed specially for Virgo and LIGO in order to make very low absorption substrates, a specific polishing protocol has been defined with a manufacturer for obtaining superpolished surfaces. Then the polished surface becomes reflecting after a coating process in which stacks of dielectric layers with alternative low and high refractive indices are deposited. The wavelength of $\lambda \sim 1.064$ μm is the best found compromise, allowing powerful light sources (Nd:YAG lasers) and low scattering losses (<1 ppm).

3.5. Planned spectral sensitivity

Owing to the preceding discussion, the overall spectral sensitivity is an envelope, resulting at low frequency (<50 Hz) from the pendulum thermal noise, in the intermediate range around 100 Hz from the mirrors internal thermal noise, and in the upper part of the spectrum from shot noise. At the resonances of the suspension wires, thin peaks appear. The foreseen sensitivity curve, after reduction of non-essential noises has the shape summarized on Fig. 3.

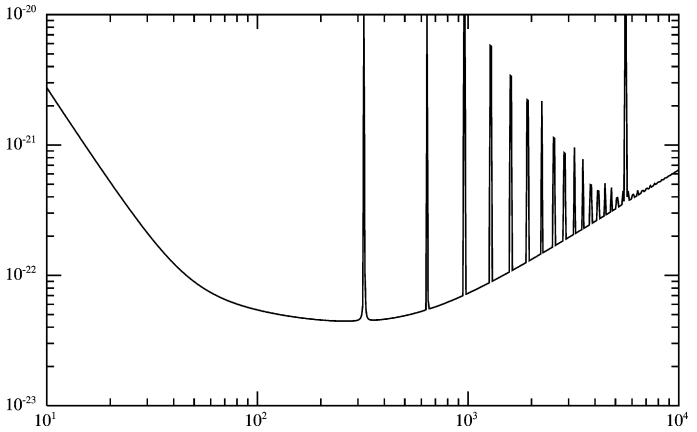

Fig. 3. Planned spectral sensitivity of Virgo.

3.6. The frequency control challenge

Frequency fluctuations of the source laser result in a specific noise on the detection channel. If the random process $\delta\nu(t)$ denotes these frequency fluctuations, the corresponding phase fluctuations on the dark fringe are

$$\delta\Phi(t) = \frac{d}{L}\frac{2\pi L}{c}\delta\nu(t) \tag{18}$$

where L is the mean length of the arms and d their difference. For a simple short Michelson interferometer, it is easy to carefully tune the arm lengths to obtain an arbitrarily low level of noise. For a long baseline interferometer with resonant cavities, the effective length $L_{\text{eff}} = (2\mathcal{F}/\pi) \times L$ depends not only on the geometrical length L of the arms, but also on the finesses of the cavities. These finesses depend in turn on the reflection coefficients of the mirrors, so that the noise level is eventually determined by the ability of technology to produce mirrors with very close reflectivities, allowing to make as symmetrical cavities as possible. We have seen that the phase shot noise LSD is

$$S_{\Phi}^{1/2}(f) = \sqrt{\frac{2\hbar\omega}{\mathcal{S}P_L}}$$

We can rewrite (18) in terms of LSD, by asking the frequency fluctuations to produce a phase noise lower than the shot noise:

$$\frac{S_{\delta\nu}^{1/2}}{\nu_L} < \frac{\lambda}{4\mathcal{F}L}\frac{\mathcal{F}}{\Delta\mathcal{F}}\sqrt{\frac{2\hbar\omega}{\mathcal{S}P_L}}$$

where $\Delta\mathcal{F}$ represents the difference between the finesses of the North and West cavities. With the same values as above, assuming $\mathcal{S}P_L \sim 1$ kW reaching the splitter, a mean cavity finesse of $\mathcal{S} \sim 50$, this is:

$$S_{\delta\nu}^{1/2} < \frac{10^{-8}}{\Delta\mathcal{F}/\mathcal{F}}\,\text{Hz}\,\text{Hz}^{-1/2}$$

with a symmetry rate of 1% for the finesse, we obtain a requirement of

$$S_{\delta\nu}^{1/2} < 10^{-6}\,\text{Hz}\,\text{Hz}^{-1/2}$$

This very strong requirement is satisfied by at least two stages of frequency control. A first stage is a servo loop using error signals by comparison of the laser frequency with a reference passive, very stable resonant cavity (long term stabilization). A second stage is a servo loop on the common mode of the two long arms (short term stabilization). The result is one the most stable oscillators in the present metrology status.

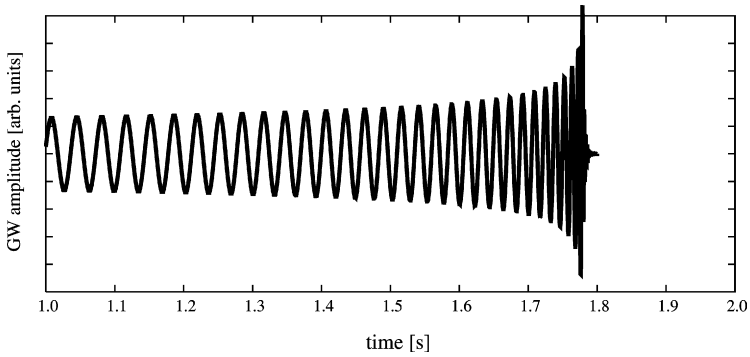

Fig. 4. Coalescence signal for two black holes.

3.7. Data analysis

The order of magnitude of the sensitivity makes likely a very poor signal to noise ratio at least in the present generation of antennas. This is why special signal processing techniques have been developed for extracting GW signature from the dominant instrumental noise background (or foreground?). Expected signals are:

- short bursts (a few ms) possibly produced by supernova or exotic cosmic string events;
- permanent waves emitted by fast pulsars having some quadrupolar moment;
- chirps emitted during the inspiral/merging/ringdown process of binary coalescence.

For the detection of binary black hole (BBH) coalescence, the common strategy of all groups is to use the matched filtering technique. It is possible to accurately describe the inspiral phase either by using the Parametrized Post Newtonian approach [14] or the Effective One Body method [15], or by numerical simulations. The result provides families of templates (each corresponding to a point in the parameter space). An example can be seen on Fig. 4 for a two 20 solar masses BBH. The signal is assumed to enter the detection band at the date at which its frequency is 20 Hz. The total duration is less than 2 s. Detection amounts to look for a correlation peak between the interferometer output and a bank of templates.

3.8. Present status

The two American LIGO antennas at Hanford (Washington) and Livingston (Louisiana) are already operating at their nominal sensitivity. The French–Italian Virgo at Cascina (Italy) comes at the end of its commissioning phase. The sensitivity is already comparable to the American antennas at high frequency (see Fig. 5).

4. LISA

LISA is the present status of a very old idea initiated in the 1970s, aiming to receive and analyze very low frequency GW from sources involving massive black holes. There is on Earth a 'wall' at a few Hz that forbids, due to direct Newtonian attraction of test mirrors by ground motions, to go to lower frequencies. The solution is therefore to be in space. LISA is an ambitious ESA/NASA joint mission which consists of three forming a triangle of 5 Mkm a side, in orbit around the Sun 50 Mkm behind the Earth. The three are optically linked by six Nd:YAG laser beams. The GW signature is read on the six Doppler data flows (beat note of the incoming light against the local oscillator). LISA is expected to fly in 2014 if the project passes a review in 2008 against a few others fundamental physics missions, and if the technological demonstrator LISA-Pathfinder is successful.

4.1. Orbital configuration

The stability of a large triangular formation on heliocentric orbits is not trivial. It can be shown (e.g. [16]) that it is possible by combining slightly elliptical, slightly inclined orbits. More specifically, let L be the inter-distance

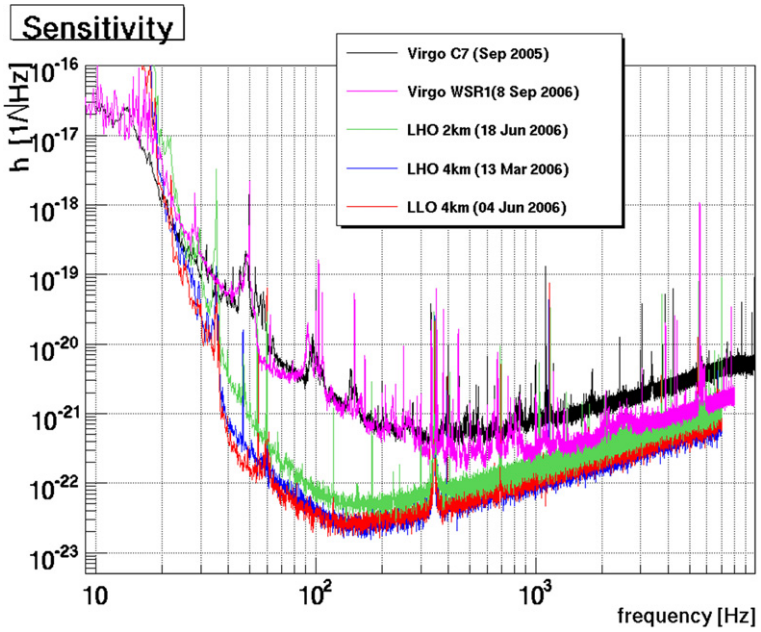

Fig. 5. Current sensitivities of LIGO and Virgo antennas.

($L \sim 5 \times 10^9$ m) and R the radius ($R \sim 1.5 \times 10^{11}$ m) of the almost circular terrestrial orbit. Let us define the small parameter $\alpha = L/2R \sim 1/60$. We can chose simultaneously for the orbit of #1 an inclination angle of ε with respect to ecliptic, and an eccentricity of e. The choice is made of

$$\varepsilon = \arctan\left[\frac{\alpha}{1+\alpha/\sqrt{3}}\right] \quad \text{and} \quad e = \sqrt{1+\frac{2\alpha}{\sqrt{3}}+\frac{4\alpha^2}{3}} - 1$$

In barycentric coordinates (centered on the Sun with (x, y) axes in the ecliptic and fixed with respect to far stars), the motion of #1 has the parametric form:

$$\begin{cases} x = R(\cos E_1 - e)\cos\varepsilon \\ y = R\sqrt{1-e^2}\sin E_1 \\ z = -R(\cos E_1 - e)\sin\varepsilon \end{cases} \tag{19}$$

where $E_1(t)$ is the so-called eccentric anomaly implicitly defined by

$$E_1 - e\sin E_1 = \Omega t$$

where $\Omega \equiv 2\pi/(1\text{ year})$. The orbits of #2 and 3 are obtained by

– Shifting by 120 degrees the eccentric anomaly, so that

$$E_i - e\sin E_i = \Omega t - (i-1)\frac{2\pi}{3} \quad (i = 1, 2, 3)$$

– Rotating the semi-major axes by 120 degrees in the (x, y) plane, so that the motions of all are parametrized by:

$$\begin{cases} X_i = x_i\cos\theta_i - y_i\sin\theta_i \\ Y_i = x_i\sin\theta_i + y_i\cos\theta_i \\ Z_i = z_i \end{cases} \tag{20}$$

where $\theta_i \equiv (i-1)\times 2\pi/3$, and where the (x_i, y_i, z_i), $i = 1, 2, 3$, are parametrized according (19) with the E_i.

The result is that the three are located in a plane making an angle of 60 degrees with respect to ecliptic, with mutual distances constant at first order in α, making a triangle rotating around its mass center with a 1 year period (see Fig. 6).

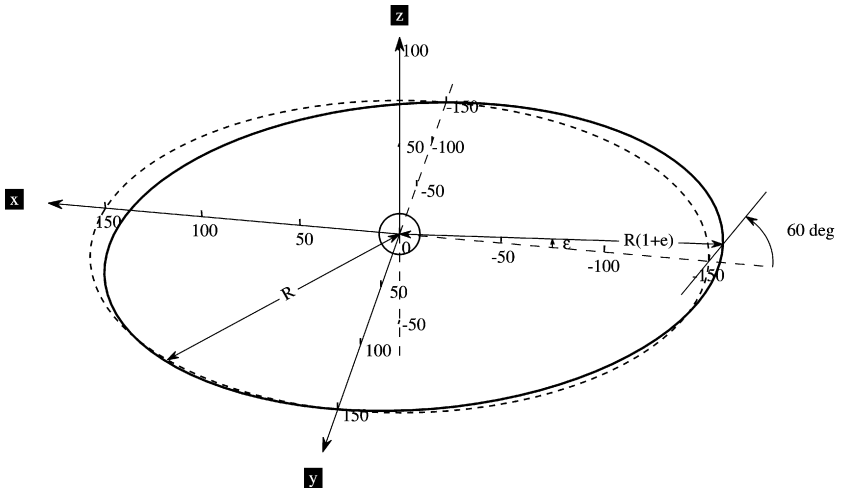

Fig. 6. Schematic of the LISA project: solid line: orbit of #1; dashed line: the Earth's orbit.

'At first order in α' means that a more accurate evaluation shows a deformation of the triangle, and inter-distances vary by about 100 000 km. It is possible to reduce this 'flexing' to less than 50 000 km by slightly increasing the 60 degrees angle (see [17]).

4.2. Drag free operation

At the level of $\Delta L/L \sim 10^{-22}$, meaning a $\Delta L \sim 5 \times 10^{-12}$ m, it is clear that perturbations caused by solar winds must be strongly rejected. It is therefore planned to operate LISA under the drag free regime. This means that the protecting shell is served on an internal reference mass by a capacitor readout system. The free falling reference mass plus the readout system form an accelerometer. This kind of accelerometer has been imagined and successfully flown by the French ONERA on several space missions [18], but here the targeted readout noise is about 3×10^{-15} m s^{-2}Hz$^{-1/2}$ in a frequency range from 10^{-4} to 10^{-1} Hz.

4.3. Data flow

In a very simplified scheme, the LISA readout system involves six phasemeters, each delivering its own data flow. If we call $C_i(t)$ $(i = 1, 2, 3)$ the instantaneous frequencies aboard the three spacecraft, the apparent Doppler measurement on board #1 for light coming from #2 is (counterclockwise) according to (10):

$$V_1 = \left[\frac{\delta\nu(t)}{\nu}\right]_{2\to 1} = \frac{H(t - \mathbf{w}.\mathbf{x}_1) - H(t - \mathbf{w}.\mathbf{x}_2 - L_3)}{2(1 - \mathbf{w}.\mathbf{n}_3)} + C_1(t) - C_2(t - L_3) + s_1(t) \tag{21}$$

(see Fig. 7); $s_1(t)$ accounts for the shot noise generated by the detection process on board #1. We take into account the fact that the triangle may be not equilateral, so that we have to deal with three different lengths L_i, $i = 1, 2, 3$. The data flows V_2, $v3$ can be obtained by cyclic permutation of the indices. For the clockwise links, we get

$$U_2 = \left[\frac{\delta\nu(t)}{\nu}\right]_{1\to 2} = \frac{H(t - \mathbf{w}.\mathbf{x}_2 - L_3) - H(t - \mathbf{w}.\mathbf{x}_1)}{2(1 + \mathbf{w}.\mathbf{n}_3)} + C_1(t - L_3) - C_2(t) + s_2(t) \tag{22}$$

The data flows U_3, U_1 are obtained by cyclic permutation of indices. It seems that the signal ($\sim 10^{-22}$), due to the huge asymmetry between the optical path of the long link (5 Mkm) and the local path ($\sim$1 m) is largely dominated by the free running frequency noises of the lasers (the C_i, $\sim$a few 10^{-14} Hz$^{-1/2}$). Fortunately, the number of data flows allows some redundancy, leading to a dramatic reduction of the noise.

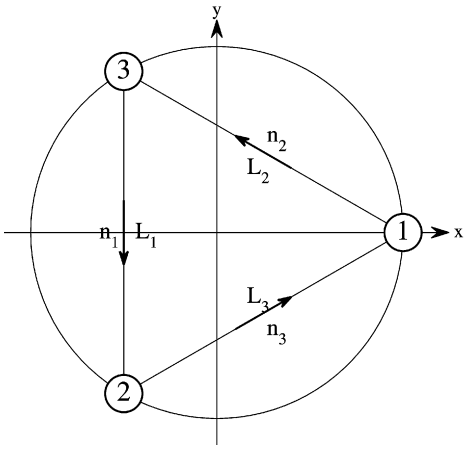

Fig. 7. Notations for the LISA geometry.

4.4. Time delay interferometry

We can define three delay operators D_i via their action on any function of time f:

$$(D_i f)(t) = f(t - L_i)$$

If we consider the part of the Doppler data due to laser noise, we can write:

$$\begin{aligned} &U_1 = D_2C_3 - C_1, \qquad U_2 = D_3C_1 - C_2, \qquad U_3 = D_1C_2 - C_3 \\ &V_1 = C_1 - D_3C_2, \qquad V_2 = C_2 - D_1C_3, \qquad V_3 = C_3 - D_2C_1 \end{aligned} \tag{23}$$

It has been remarked that some combinations of the U_i, V_i give an identically zero result, and can be regarded as noise cancelling. Use of such noise cancelling combination was proposed by M. Tinto [19] and called 'Time Delay Interferometry' (TDI). The algebraic structure of TDI has been found and explained in [7]. The simplest example is found by considering the C_i U_i and the V_i as vectors **C**, **U**, **V** and the delay operators D_i as the components of a vector operator **D**. The sum $\mathbf{U} + \mathbf{V}$ has the algebraic signature of a curl:

$$\mathbf{U} + \mathbf{V} = \mathbf{D} \times \mathbf{C}$$

It is now clear that the 'divergence' of $\mathbf{U} + \mathbf{V}$ is identically zero, so that

$$\mathbf{D}.(\mathbf{U} + \mathbf{V}) = 0 \quad \Rightarrow \quad \sum_{i=1}^{3} D_i U_i + \sum_{i=1}^{3} D_i V_i = 0$$

Each noise cancelling combination y can thus be represented by a 6-uple $Y = (p_i, q_i)$ of polynomial in the formal variables D_i, acting on the data 6-uple $U = (V_i, U_i)$:

$$y = \langle Y|U\rangle = \sum_{i=1}^{3}(p_i V_i + q_i U_i)$$

The basis of TDI is the set $\mathcal{S}$ of all Ys. It has been shown [7] that $\mathcal{S}$ has the algebraic structure of a first module of syzygies on the ring of formal polynomials. This means that any element of $\mathcal{S}$ can be obtained by a linear combination whose coefficients are polynomials in D_i, of generators of $\mathcal{S}$. A generating part of $\mathcal{S}$ has been found by [19]:

$$\zeta = (\mathbf{p}, \mathbf{q}) = (D_1, D_2, D_3, D_1, D_2, D_3)$$

already found above, and

$$\alpha = (1,\ D_3,\ D_1D_3,\ 1,\ D_1D_2,\ D_2)$$

with its two successive circular permutations (of indices and of locations in the sub-3-uples):

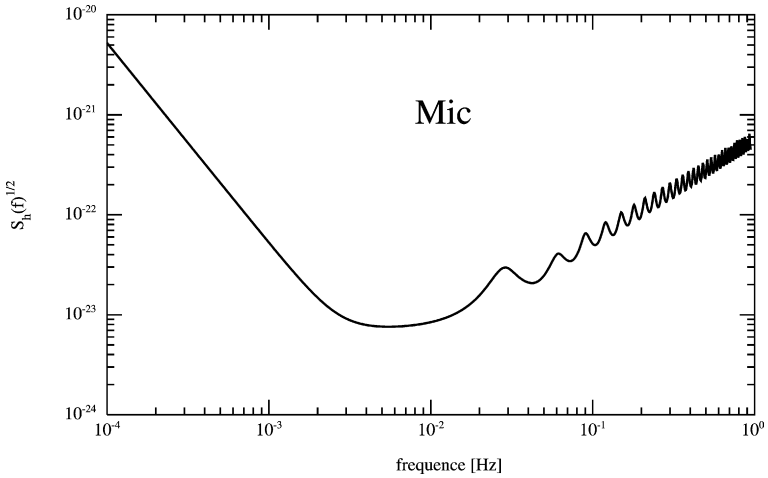

Fig. 8. Mean spectral sensitivity of LISA for the 'Michelson' TDI combination.

$$\beta = (D_1 D_2,\ 1,\ D_1,\ D_3,\ 1,\ D_2 D_3)$$

$$\gamma = (D_2,\ D_2 D_3,\ 1,\ D_1 D_3,\ D_1,\ 1)$$

Any combination of α, β, γ applied to the data 6-uple **U** is thus laser noise free. It can be shown that the same combination is still sensitive to GW. Generator ζ (often called 'symmetric Sagnac') strongly attenuates the GW signals at low frequency. There is no hope, however, of suppressing the shot noise nor the noise coming from the accelerometer readout system, because those are purely local noises (not transmitted to other with some delay). The global sensitivity curve for a typical TDI combination ('Michelson') is shown on Fig. 8: it assumes one year integration time for a permanent source, with a signal to residual noise ratio of 5, and an average on the angular coordinates of the source. In reality, the situation is more complex because there are six lasers, not three, and the propagation times between two are not reciprocal, due, for instance, to the Sagnac effect in rotating frames, and even variable in time due to the flexing effect. However, the preceding method remains valid in principle, up to improvements [20].

4.5. Data analysis

Owing to the low frequency domain of sensitivity, the sampling frequency may be taken at a fraction of a Hz, so that the flow of data down to Earth is consistent with the bandwidth of the microwave link. A preprocessing by TDI generators is necessary, which implies a good knowledge of the instantaneous inter-distances. Depending on the kind of source to be studied, several strategies may be developed.

A major point is the existence of a foreground of GW noise generated by the population of galactic compact binaries (involving neutron stars, white dwarfs, black holes) whose orbital frequencies (times 2) fall within the detection band of LISA. The GW amplitude resulting from all these monochromatic sources is analogous to a stochastic background. These objects are a huge number (e.g. $\sim 10^8$ white dwarf binaries, see [21]). All of these produce a so-called confusion noise the spectral density of which is dominant at very low frequency (from 0.1 to 1 mHz). For detecting a particular binary, it is possible to find optimal combinations of the generators [22] and even combinations giving a zero result, allowing us to selectively suppress known sources [23,22] for a 'coronographic' operation of LISA.

The signals generated by or around black holes are of two types:

– Stellar class objects orbiting supermassive black holes have complex inspiralling trajectories ending by a capture. The models for such events are called Extreme Mass Ratio Inspirals (EMRI). The GW emitted during EMRI have a complex frequency structure [24]. These models depends on a number of parameters making difficult a matched filtering approach. Moreover, situations may happen in which several bodies are involved resulting in a perturbed process escaping the 'simple' model. Time-Frequency methods based on wavelet transforms seem a right tool.

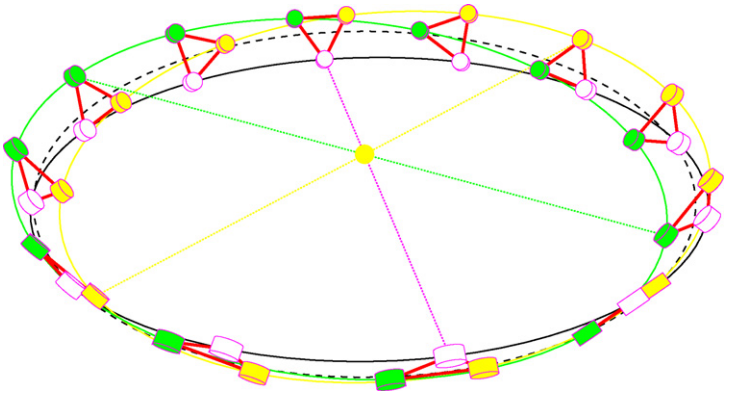

Fig. 9. Simulation of the orbital evolution of LISA.

– Supermassive Binary Black Holes (SMBBH) are expected to inspiral on a long time period. The final phase could be observed during several years of LISA operation. A matched filtering approach is possible, and Time-Frequency methods as well.

4.6. Simulation

The closest date of launch of the mission being 2014, the preparation of the Data Analysis System must be developed and tested with synthetic data. Two data simulators have been coded in the United States and one in France:

– Synthetic LISA at the Jet Propulsion Laboratory (Pasadena, California) [25];
– The LISA Simulator at Montana University [26];
– LISACode by LISA-France (APC, observatoire de la côte d'Azur) [27] (see Fig. 9).

The simulators compute the orbital motion (20) of each and the corresponding transfer function (21), (22) for the GW signals. The GW amplitudes for several kind of sources and angular locations are read from files and the result is given in terms of TDI generators.

5. Conclusion

Gravitational Wave Astronomy has now entered its technological phase after more that thirty years of R&D. The ground based antennas are about to form a network. The space mission LISA is now almost defined. Exploitation of these large instruments require more young searchers. We hope that the present short presentation will be regarded as a first introduction to this new field.

References

[1] K.S. Thorne, in: S.W. Hawking, W. Israel (Eds.), 300 Years of Gravitation, Cambridge Univ. Press, 1987.
[2] J. Weber, in: H.-Y. Chiu, W.F. Hoffmann (Eds.), Gravitation and Relativity, W.A. Benjamin Inc., New York, Amsterdam, 1964.
[3] J.-Y. Vinet, Ann. Inst. Henri Poincaré XXX (3) (1979) 251.
[4] L. Baggio, et al., Phys. Lett. 95 (2005) 081103.
[5] P. Astone, et al., Class. Quant. Grav. 23 (2006) S57–S62.
[6] A. de Waard, et al., in: Proceedings of the 6th Amaldi Conference on Gravitational Wave, Okinawa, Japan, 2005; J. Phys., submitted for publication.
[7] S.V. Dhurandhar, R.K. Nayak, J.-Y. Vinet, Phys. Rev. D 65 (2002) 102002.
[8] R. Drever, in: N. Deruelle, T. Piran (Eds.), Gravitational Radiation, North-Holland, 1983, p. 321.
[9] Yu. Levin, Phys. Rev. D 57 (1998) 659.
[10] E. D'Ambrosio, Phys. Rev. D 67 (2003) 102004.
[11] J.-Y. Vinet, Class. Quant. Grav. 22 (2005) 1395.
[12] J. Agresti, et al., LIGO technical documents, http://www.ligo.caltech.edu.

[13] B. Mours, E. Tournefier, J.-Y. Vinet, Class. Quant. Grav. (September 2006), in press.
[14] L. Blanchet, Phys. Rev. D 72 (2005) 044024.
[15] A. Buonanno, T. Damour, Phys. Rev. D 59 (1999) 084006.
[16] S. Dhurandhar, R. Nayak, S. Koshti, J.-Y. Vinet, Class. Quant. Grav. 22 (3) (2005) 481–487.
[17] R. Nayak, S. Koshti, S. Dhurandhar, J.-Y. Vinet, Class. Quant. Grav. 26 (2006) 1763–1778.
[18] P. Touboul, A. Bernard, C. R. Acad. Sci. Paris Sér. IV (2001) 1271.
[19] M. Tinto, J. Armstrong, F. Estabrook, Astrophys. J. 527 (1999) 814–826.
[20] R. Nayak, J.-Y. Vinet, Phys. Rev. D 70 (2004) 102003.
[21] G. Nelemans, L. Yungelson, S. Portegies Zwart, Astron. Astrophys. 375 (2001) 890–898.
[22] R. Nayak, S. Dhurandhar, A. Pai, J.-Y. Vinet, Phys. Rev. D 68 (2003) 122001.
[23] M. Tinto, S. Larson, Class. Quant. Grav. 22 (10) (2005) S531–S535.
[24] S. Hughes, Class. Quant. Grav. 18 (2001) 4067–4073.
[25] http://www.vallis.org/syntheticlisa/.
[26] http://www.physics.montana.edu/lisa/.
[27] http://www.apc.univ-paris7.fr/SPIP/article.php3?id_article=164.